Digital Predistortion Linearization For Carrier Aggregation And Wide Bandwidth

R. Zepeda-Puebla

Abstract— Development of a digital predistortion (DPD) linearization system of a power amplifier (PA) for carrier aggregation (CA) and wide-bandwidth, radio-frequency (RF) signals is presented. A methodology for optimizing parameter values in a Volterra-based, cubic spline interpolation model is proposed. The optimized models and the DPD system itself are validated in a RF-sampling, FPGA-based experimental testbed. Performance is evaluated using the normalized mean square error (NMSE) and the adjacent-channel power ratio (ACPR) figures of merit for three different excitations of varying number of component carriers (CCs) and total bandwidth. NMSE is found to improve by 33 dB on average when compared to the case where no DPD is applied, while ACPR improves by 15.6 dBc on average for the same comparison.

Index Terms— carrier aggregation (CA), cubic spline (CS), digital predistortion (DPD), linearization, power amplifier (PA), radio frequency (RF), wireless communications.

1 INTRODUCTION

High power efficiency is an essential requirement in modern wireless communications systems that has created significant challenges in the design of the RF front-end, where the Power Amplifier (PA) is responsible for most of the power consumption. This necessity has led to important developments in PA architectures (e.g. Doherty [1], [2], and Chireix [3], [4]) where highly efficient designs have been achieved. However, high power efficiency comes with a tradeoff: a non-linear characteristic that generates spectral regrowth in the form of intermodulation distortion (IMD) terms. Furthermore, even if the PA in question is capable of operating in a linear region, the amplitude- and phase-modulated signals used in high data rate connections possess high peak to average power ratio (PAPR), which means the amplifier must operate close to saturation in order to maintain its high power efficiency.

Digital predistortion (DPD) linearization is a robust and highly accurate solution to the aforementioned tradeoff in PA design. Its foundation is PA behavioral modeling [5], which offers significant advantages over physical models: the amplifier can be considered as a black box and only the excitation and the observed "behavior" (in the form of the digitally-sampled output to the PA) are relevant to the problem. Comparatively, a physical model requires a great amount of information about the actual circuit, every component, and every mechanism that affects the response of the PA. What this means for DPD is execution times are fast and can even be implemented on an application-specific integrated circuit (ASIC) or a field-programmable gate array (FPGA) for portability and cost effectiveness.

An important aspect of DPD and PA behavioral modeling is memory effects, of which two variations exist: long-term and short-term memory effects. Long-term memory effects are due to temperature phenomena inside the transistors, such as current traps and self-heating, and happen slowly enough that the model can "adapt" to them by calculating new coefficients. Short-term memory effects are due to the inertia of the response of the circuit to the modulated signal and become more latent with an increasing bandwidth; they must be handled as part of the model by taking into account previous values of the sampled signals.

The behavioral models employed in the DPD problem are based on the Volterra series approach to model a dynamic, non-linear system with non-linear memory. They consist of building a set of non-linear basis functions so that taking a linear combination of them represents the PA characteristic accurately enough that IMD terms can be successfully canceled from the frequency spectrum of the linearized output to the PA.

Perhaps the most popular Volterra-based model that is used to linearize a radio frequency (RF) power amplifier is the memory polynomial (MP) [6], [7], [8], [9]. Although it can be sufficient in linearizing the non-linear characteristic, it has the particular disadvantage of becoming numerically unstable too quickly, as increasing the polynomial order in an effort to reduce modeling errors translates into an ill-conditioned regression matrix, as indicated by the condition number of said matrix.

Improved performance of the DPD process can be achieved by a different model, based on cubic spline (CS) basis functions [10], [11]. The CS model shows a significant reduction of the condition number of the regression matrix. This is due to its piece-wise approach to represent the range of the behavior that it is trying to model. Other improvements when compared to the MP model come in the form of a reduced number of coefficients (which helps to reduce extraction times) that even though smaller in number, yield better model accuracy, as indicated by the normalized mean-square error (NMSE), and an improved adjacent-channel power ratio (ACPR), which measures the effectiveness of the IMD suppression by comparing the spectral content of the band of the output signal to the spectral content on either side of the band. For these reasons, the CS model will be used in this paper's implementation of a DPD linearization system for carrier aggregation (CA) and wide signal bandwidth.

CA is a technique where multiple component carriers (CCs) can be used concurrently to create a composite signal of broader bandwidth. CA is one of the ways the increasing demand for higher data rates can be met in the latest (and last) releases of the 4G-LTE (4th-generation Long-Term Evolution)

standard for wireless communications, along with 4x4 MIMO (4x4 multiple input, multiple output) and 256-QAM (256-Quadrature Amplitude Modulation) [12].

Even as 4G sun-sets, to be replaced by 5G-NR (5th-generation New Radio) eventually, it continues to be in billions of users' hands around the world, and so a DPD solution for this type of signals will stay relevant for years; until the coverage, the performance, and the user base of 5G, all get to a point where it becomes the dominant technology.

The remainder of this paper is structured as follows: Section 2 describes the theory and mathematical equations of the DPD problem; Section 3 presents simulation results where model performance is evaluated for different sets of parameters in the model and signals of one, three, and five CCs; Section 4 includes experimental validation of the DPD system; lastly, Section 5 states conclusions and final remarks.

2 Modeling the Linearization System

This section describes the necessary theory and mathematical equations for the development of the DPD linearization system presented in this paper, starting with the fundamentals of modeling a dynamic system, continuing with the Volterra series and Volterra-based approaches to representing non-linear behavior, and ending with the derivation of the DPD expressions.

A causal, linear system with memory can be described in terms of its impulse response $h(\tau)$ through a convolution integral:

$$y(t) = \int_{-\infty}^{+\infty} h(\tau)\, x(t-\tau)\, d\tau\,, \tag{1}$$

where $x(t)$ and $y(t)$ are the input and output to the system, respectively.

On the other hand, a memory-less, non-linear system can be described through a power series:

$$y(t) = \sum_{j=1}^{\infty} a_j\, [x(t)]^j\,, \tag{2}$$

where a_j are the coefficients of the power series, and $x(t)$ and $y(t)$ are the input and output to the system, respectively.

The Volterra series approach, the most exhaustive way of modeling a non-linear system with non-linear memory, with input $x(t)$ and output $y(t)$, can be obtained by combining (1) and (2), as

$$y(t) = \sum_{p=1}^{\infty} y_p(t)\,, \tag{3}$$

where $y_p(t)$ is the p-th term of the infinite sum that composes output, and is given by

$$y_p(t) = \int_{-\infty}^{+\infty} \dots \int_{-\infty}^{+\infty} h_p(\tau_1, \dots, \tau_p) \prod_{q=1}^{p} x(t-\tau_q)\, d\tau_q\,, \tag{4}$$

where $h_p(\tau_1, \dots, \tau_p)$ is the p-th order, multidimensional impulse response.

In the case of PA behavioral modeling and DPD modeling, the signals involved are digital signals, which means (4) needs to become finite and discrete:

$$y(n) = \sum_{p=1}^{P} \sum_{m_1=0}^{M-1} \dots \sum_{m_k=0}^{M-1} h_p(m_1, \dots, m_p) \prod_{q=1}^{p} x(n-m_q)\,, \tag{5}$$

where P is the non-linearity order and M is the memory depth.

As indicated by (5), the number of parameters in the Volterra series increases steeply with increasing non-linearity order and memory depth; due to this high complexity, its application was limited to weakly non-linear systems only for a long time, until more efficient, Volterra-based models were developed. Such models consist of setting a reduced memory depth and choosing a reduced set of non-linear basis functions of the input.

A commonly used, Volterra-based model in PA behavioral modeling and DPD modeling is the memory polynomial (MP) model, given by

$$y(n) = \sum_{m=0}^{M-1} \sum_{k=0}^{K-1} x(n-m) \cdot |x(n-m)|^{2k} \cdot c_{m,k}\,, \tag{6}$$

where $x(n)$ and $y(n)$ are the input and output signals to the PA, respectively; K sets the polynomial order to $2(K-1)$, M is the memory depth, and $c_{m,k}$ are the coefficients of the model.

As previously mentioned, the cubic spline (CS) model has proven a better alternative to (6) for its local, third-order polynomials rather than a single, global, high-order one; as such, this is the model to be implemented in the DPD system in what follows.

The CS model is given by

$$y(n) = \sum_{m=0}^{M-1} \sum_{i=1}^{N_b} \phi_i(n)\, x(n-m) \cdot c_{m,i}\,, \tag{7}$$

where $x(n)$ is the input signal to the PA, $y(n)$ is the output signal, N_b is the number of nodes, M is the memory depth, $c_{m,i}$ are the coefficients of the model and $\phi_i(n)$ are the cubic spline basis functions.

The functions $\phi_i(n)$ are constructed by performing cubic spline interpolation [13] of $|x(n)|^2$ over a vector of size N_b where the i-th element is equal to one and all other elements are zero.

In matrix form, (7) can be written as

$$\vec{y} = \boldsymbol{A}(\vec{x}) \cdot \vec{c}_{PA}\,, \tag{8}$$

where $\vec{y}$ is a $N \times 1$ vector, $\boldsymbol{A}$ is a $N \times (N_b \cdot M)$ matrix, and $\vec{c}_{PA}$ is a $(N_b \cdot M) \times 1$ vector.

The least-squares solution to the system in (8) is given by the well-known

$$\hat{c}_{PA} = (\boldsymbol{A}^H\, \boldsymbol{A})^{-1}\, \boldsymbol{A}^H\, \vec{y}\,, \tag{9}$$

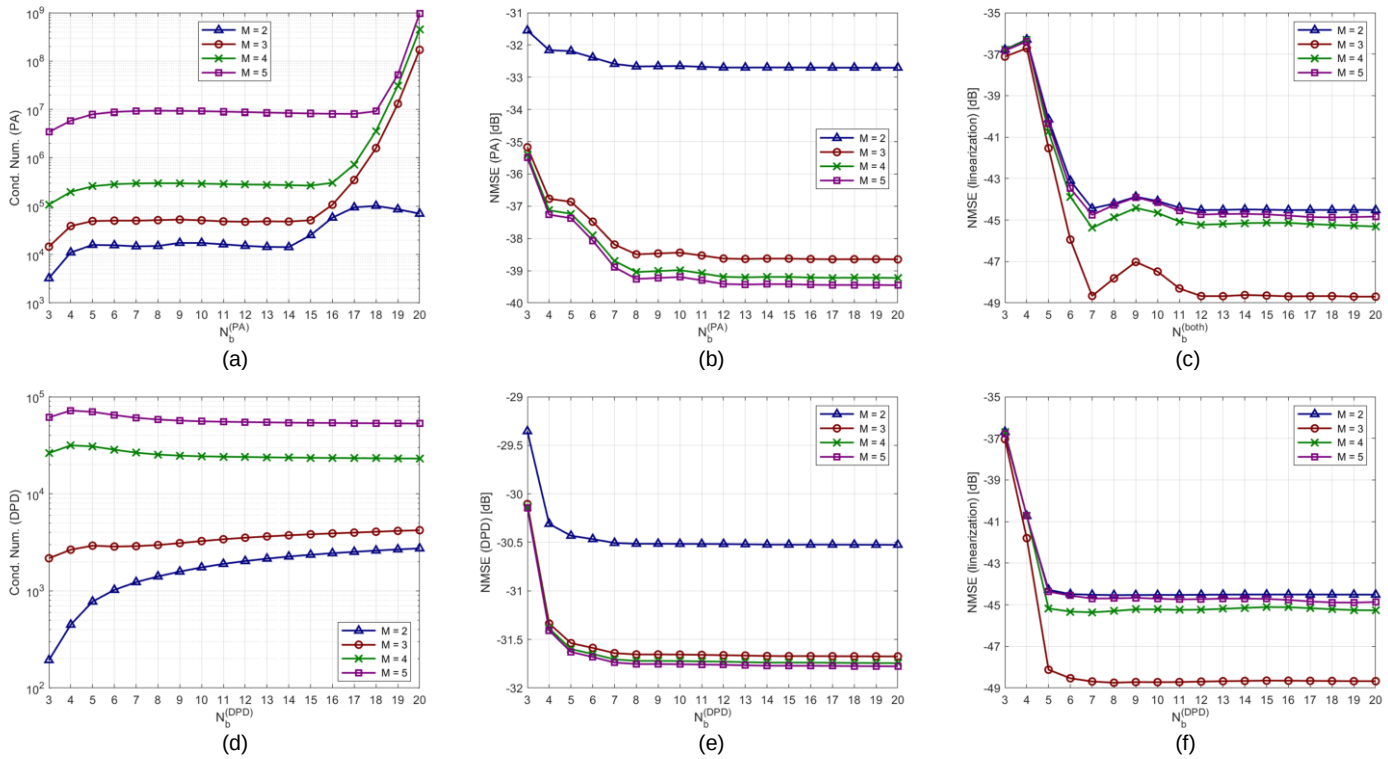

Fig. 1. Simulation results for a 5-carrier LTE signal of 100 MHz in total bandwidth: (a) condition number for the regression matrix in the PA model, (b) NMSE for the PA model, (c) NMSE for the linearization while sweeping the number of nodes for both PA and DPD, (d) condition number for the regression matrix in the DPD model, (e) NMSE for the DPD model, and (f) NMSE for the linearization with a fixed number of nodes for the PA model.

where $\hat{c}_{PA}$ are the estimated coefficients, and the subscript H denotes Hermitian transpose.

From the estimated coefficients $\hat{c}_{PA}$, a model of the output can be calculated:

$$\hat{y}_{model} = \boldsymbol{A}(\vec{x}) \cdot \hat{c}_{PA} \,. \tag{10}$$

By swapping the input and output in the PA behavioral model from (8), the DPD model can be obtained:

$$\vec{x} = \boldsymbol{A}(\vec{y}) \cdot \vec{c}_{DPD} \,, \tag{11}$$

and subsequently solved:

$$\hat{c}_{DPD} = (\boldsymbol{A}^H \boldsymbol{A})^{-1} \boldsymbol{A}^H \vec{x} \,. \tag{12}$$

Similarly to (10), a model of the input can be computed from the estimated coefficients $\hat{c}_{DPD}$ from the DPD model:

$$\hat{x}_{model} = \boldsymbol{A}(\vec{y}) \cdot \hat{c}_{DPD} \,. \tag{13}$$

The predistortion signal $\vec{z}$ that will replace $\vec{x}$ in order to linearize the PA, is given by

$$\vec{z} = \boldsymbol{A}(\vec{x}) \cdot \hat{c}_{DPD} \,. \tag{14}$$

Finally, a linear output signal to the PA can be computed in simulation through

$$\vec{y}_{linear} = \boldsymbol{A}(\vec{z}) \cdot \hat{c}_{PA} \,. \tag{15}$$

Experimentally, only (12) and (14) are needed to complete the linearization process. However, (9) and (15) are still very much useful; with them, along with (10), (12), and (13), the parameters of the CS model will be intelligently chosen in the next section.

3 Simulation Results

Before moving on and start testing the DPD system experimentally, it is worth finding the optimal parameters of the CS model (namely, the number of nodes and memory depth) for both the PA model and the DPD model, and for each of the signals that will be exciting the PA. To accomplish this, a specific methodology will be proposed in what follows, drawing from the information generated in simulation.

Simulating the DPD system is especially useful for sweeping parameters and finding the values that yield best results. Instead of generating the predistorted signal $\vec{z}$ and sending it to the PA, it can be used in the PA model, as indicated by (15). This allows for relatively quick predictions of what will happen for each set of parameters, rather than taking measurement after measurement to make adjustments.

To characterize performance of the model, three figures of merit can be used: the condition number of the regression matrix, the normalized mean square error (NMSE), and the adjacent-channel power ratio (ACPR).

The condition number of the regression matrix ($\boldsymbol{A}^H \boldsymbol{A}$) in (9) and (12), is simply defined as the ratio of its largest singular

value to its smallest.

The NMSE for comparing two discrete signals $x(n)$ and $y(n)$ is calculated as

$$NMSE_{(x,y)} = 10\log_{10}\left(\frac{\sum_n |x(n)-y(n)|^2}{\sum_n |x(n)|^2}\right). \quad (16)$$

Three variations of the NMSE figure will become useful: First, to evaluate the accuracy of the PA model, $NMSE_{(y,y_{model})}$ will be computed (and indicated in plots as $NMSE(PA)$ for legibility reasons). Secondly, the accuracy of the DPD model will be indicated by $NMSE_{(x,x_{model})}$ (or $NMSE(DPD)$ in plots). Thirdly, the joint performance of the two models will be measured through the computation of $NMSE_{(x,y_{linear})}$ (or $NMSE(linearization)$ in plots).

An NMSE figure that is lower than –30 dB indicates good enough accuracy of the corresponding model.

ACPR is usually computed twice, one for either side of the channel, to compare the power content of the channel to the content of the adjacent bands. It is given by

$$ACPR = 10\log_{10}\left(\frac{\sum_{f_{adj}} |PSD_y(f_{adj})|}{\sum_{f_{ch}} |PSD_y(f_{ch})|}\right), \quad (17)$$

where $PSD_y(f_{adj})$ is the frequency-dependent power density function (PSD) of one of the adjacent bands of signal y, and $PSD_y(f_{ch})$ is the frequency-dependent power density function (PSD) of the channel band. Index f_{adj} covers frequency interval

$$\left(-f_{offset} - \frac{BW_{adj}}{2}\right) \le f_{adj} \le \left(-f_{offset} + \frac{BW_{adj}}{2}\right), \quad (18)$$

for the lower adjacent band, and

$$\left(f_{offset} - \frac{BW_{adj}}{2}\right) \le f_{adj} \le \left(f_{offset} + \frac{BW_{adj}}{2}\right), \quad (19)$$

for the upper adjacent band; BW_{adj} is the bandwidth of the adjacent bands, and f_{offset} defines the location of the adjacent bands. Finally, index f_{ch} covers the frequency interval of the channel, of bandwidth BW_{ch}:

$$-\frac{BW_{ch}}{2} \le f_{ch} \le \frac{BW_{ch}}{2}. \quad (20)$$

The mask requirement for the spectral content of the linearized output dictates the ACPR figure will need to be lower than –45 dBc for each of the two adjacent bands.

Fig. 1 shows simulation plots for a sweep of the number of nodes N_b from 3 to 20, and of the memory depth M from 2 to 5, in the PA and DPD models, for a 5-carrier LTE input signal $\vec{x}$ of 20-MHz CCs and 100 MHz in total bandwidth, and a corresponding output signal $\vec{y}$ captured experimentally.

It was found through multiple tests that looking at $NMSE(DPD)$ first is the best starting point: these simulation results show that $M = 3$ has the largest improvement over the previous curve for $M = 2$, whereas $M = 4$ and $M = 5$ show little improvement over $M = 3$. As for $N_b^{(DPD)}$, increasing its value improves $NMSE(DPD)$ gradually, until it plateaus at $N_b^{(DPD)} = 8$.

Now, let us look at $NMSE(PA)$. Memory depth follows a similar behavior than before in the DPD model; $M = 3$ is the sweet spot again. The number of nodes saturates the error in the PA model at $N_b^{(PA)} = 13$.

The plots for the condition number of the PA model ($Cond.Num.(PA)$) and the DPD model ($Cond.Num.(DPD)$) confirm $M = 3$ as the best choice, since $M = 4$ and $M = 5$ increase these figures too much and might result in numerical instability. On the other hand, the difference between the $M = 2$ and the $M = 3$ curves might be worth the risk, because of the benefits seen in both error figures previously inspected.

In Figs. 1 (c) and (f), two different plots for $NMSE(linearization)$ are displayed. The first one was generated while sweeping N_b in both the PA model, and the DPD model; the second one was generated for a fixed $N_b^{(PA)} = 13$ in the PA model, while sweeping $N_b^{(DPD)}$. This is because the $NMSE(linearization)$ curves in the first plot show a spike before settling around $N_b^{(both)} = 13$, and so given that this coincides with the point where $NMSE(PA)$ settles, and before $Cond.Num.(PA)$ starts to climb, it makes sense to decide on $N_b^{(PA)} = 13$ as the final value for the PA model. The second plot confirms this as the right decision, as the spike disappears. Moreover, the curve for $M = 3$ in the second plot supports all previous evidence that this value for memory depth should be the winner. Lastly, $N_b^{(DPD)} = 8$ is also confirmed in the second plot as a good value for the number of nodes in the DPD model.

ACPR plots were omitted from Fig. 1 since they do not show much variation for different memory depth; the curves practically overlapped and were not visually attractive. Furthermore, the optimal values for the number of nodes that were chosen before are good enough for this figure of merit as well. In other words, the two condition numbers and the various NMSE figures should be used for finding the optimal values, whereas the ACPR should only be checked for confirmation, and verified to be lower than the mask requirement of –45 dBc on either side of the channel.

The same workflow was followed to find the best parameters for 3- and 1-carrier LTE signals. The same values chosen for the 5-carrier case were verified as appropriate for the other two. Next, simulation results will be validated for all three signals experimentally in the next section.

4 Experimental Results

Having found a methodology for optimizing parameter values in simulation, the DPD linearization system can now be tested experimentally. For this purpose, an RF-sampling transceiver board was used in tandem with an FPGA-based data converter board, both from Texas Instruments, and a PC.

In this setup, the excitation is generated and formatted in the PC, handled by the FGPA, then delivered to the PA by means of a digital to analog converter (DAC) integrated circuit that takes in a 491.52-MSPS baseband signal, sets the carrier frequency to 3.5 GHz through a numerically-controlled oscillator (NCO), and interpolates by 18x to deliver a 8847.36 MSPS output.

In the observation path, an analog to digital converter

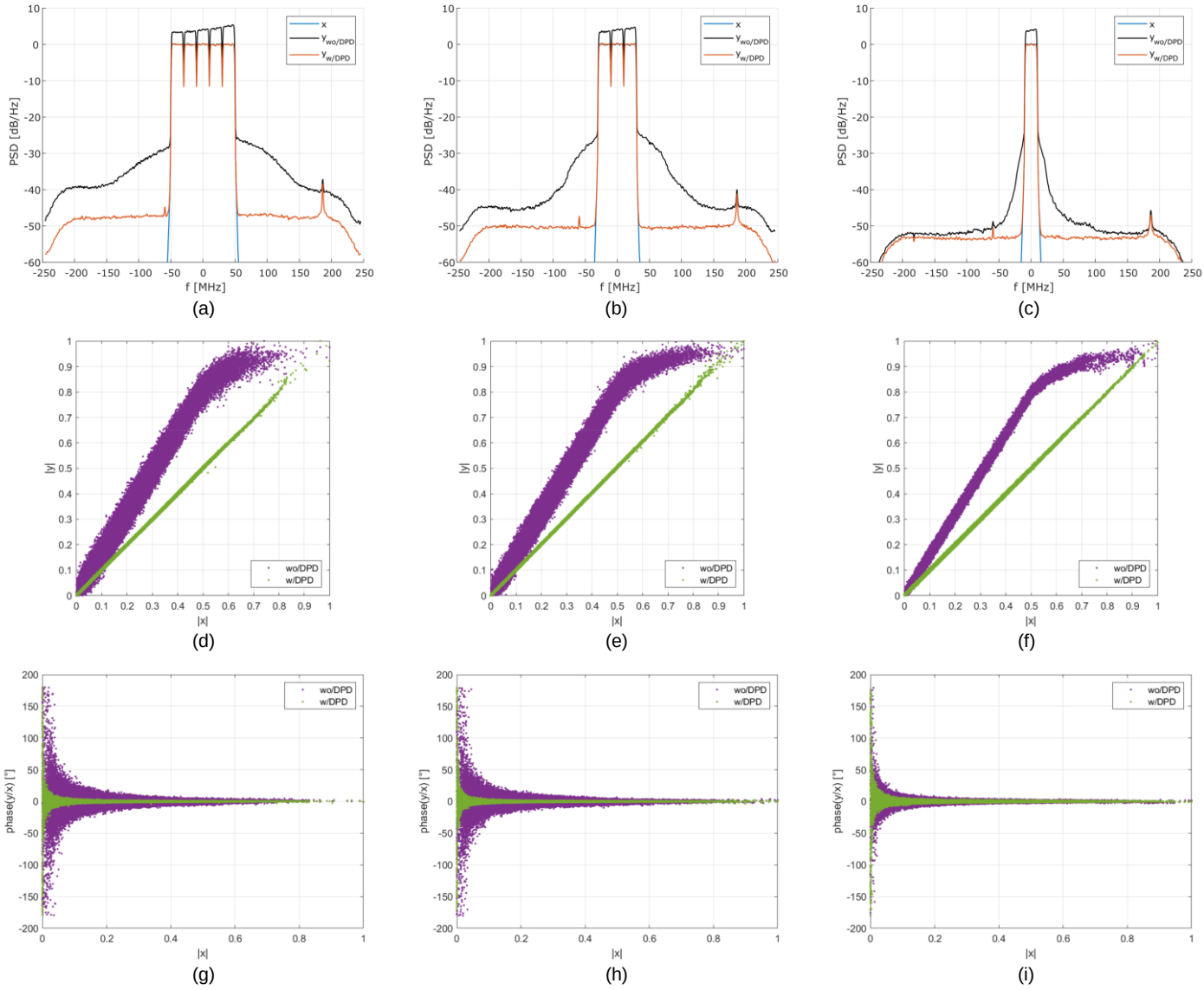

Fig. 2. Experimental results for the DPD linearization system for CA and wide bandwidth: (a) PSD frequency spectrum of a 5-carrier LTE signal of 100 MHz in total bandwidth, (b) PSD frequency spectrum of a 3-carrier LTE signal of 60 MHz in total bandwidth, (c) PSD frequency spectrum of a 1-carrier LTE signal of 20 MHz in bandwidth; (d) AM/AM plot for the 5-carrier signal, (e) AM/AM plot for the 3-carrier signal, (f) AM/AM plot for the 1-carrier signal; (g) AM/PM plot for the 5-carrier signal, (h) AM/PM plot for the 3-carrier signal, (i) AM/PM plot for the 1-carrier signal.

(ADC) integrated circuit samples the signal at 2949.12 MSPS, sets the center frequency to 3.5 GHz in the third Nyquist zone through a NCO, and a 6x decimation step is performed to send a 491.52-MSPS capture to the FPGA, which in turn sends it to the PC.

Experimental results for 5-, 3-, and 1-carrier LTE signals are presented in Fig. 2 for two different scenarios each: the PA without DPD (wo/DPD), and the linearized PA with DPD (w/DPD). In the wo/DPD case, the output of the PA is captured in the ADC, receiver path; this is signal $\vec{y}$ previously used in simulation to optimize model parameter values. In the linearization step, w/DPD, the predistorted signal $\vec{z}$ replaces $\vec{x}$ as the input signal to the PA, and a new, measured $\vec{y}_{linear}$ is captured. This is in contrast to the simulation $\vec{y}_{linear}$ that can be computed through (15).

Figs. 2 (a), (b), (c) correspond to the PSD frequency spectrum of each of the excitations. In these, the black line shows the spectral regrowth in $\vec{y}$, which is then suppressed in the measured $\vec{y}_{linear}$ in red line, through DPD.

Figs. 2 (d), (e), (f) display the amplitude modulation relationship (AM/AM) that compares the normalized magnitudes of the input and output signals to the PA, without and with DPD. The non-linear gain and memory effects can be assessed from the purple points, while the green plot indicates successful linearization of the PA output as these points come close to a 45-degree straight line.

TABLE 1
NMSE AND ACPR OF THE DPD LINEARIZATION SYSTEM

Scenario	NMSE [dB]	ACPR (lower) [dBc]	ACPR (upper) [dBc]
5-c LTE wo/DPD	–4.13	–32.94	–30.54
5-c LTE w/DPD	–38.37	–46.31	–45.90
3-c LTE wo/DPD	–4.42	–30.84	–29.37
3-c LTE w/DPD	–37.09	–47.41	–49.74
1-c LTE wo/DPD	–4.89	–35.55	–34.7
1-c LTE w/DPD	–37.11	–48.82	–49.62

Figs. 2 (g), (h), (i) show the amplitude modulation versus phase modulation relationship (AM/PM) of the normalized input and output signals. In these, the green points come closer to the 0-degree horizontal line, when compared to the purple points, to indicate successful linearization.

Finally, the performance of the DPD linearization process can be quantified by computing the NMSE of $\vec{x}$ versus the measured $\vec{y}_{linear}$, and ACPR for the lower and upper side bands of the measured $\vec{y}_{linear}$, for an offset of 20-MHz, since this is the bandwidth of the CCs in the three excitations. These measured results are summarized in TABLE 1; they indicate an average improvement of 33 dB for the NMSE and an average difference of 15.6 in ACPR.

5 CONCLUSIONS

In this paper, a DPD linearization system for CA and wide-bandwidth 4G-LTE signals has been implemented using Volterra-based, cubic spline models.

The optimal parameter values for the models were found in simulation and a work flow for this process has been proposed. These results have been validated experimentally using a RF transceiver and a data converter modules through a visual assessment of PSD spectrum, AM/AM, and AM/PM plots, and linearization performance has been quantified to meet and exceed the requirements of a NMSE lower than –30 dB, and an ACPR lower than –45 dBc.

ACKNOWLEDMENTS

The author would like to thank the Consejo Nacional de Ciencia y Tecnología (CONACyT) for awarding the fellowship during his graduate program, the Universidad Nacional Autónoma de México (UNAM), and the Ohio State University (OSU). This work was supported in part by DGAPA PAPIIT under Grant IN118719.

REFERENCES

[1] W. H. Doherty, "A new high efficiency power amplifier for modulated waves", *Proc. Inst. Radio Eng.*, vol. 24, no. 9, pp. 1163–1182, Sep. 1936.
[2] V. Camarchia, M. Pirola, R. Quaglia, S. Jee, Y. Cho and B. Kim, "The Doherty power amplifier: Review of recent solutions and trends," *IEEE Trans. Microw. Theory Tech.*, vol. 63, no. 2, pp. 559–571, Feb. 2015.
[3] H. Chireix, "High power outphasing modulation," *Proc. Inst. Radio Eng.*, vol. 23, no. 11, pp. 1370–1392, Nov. 1935.
[4] T. Barton, "Not just a phase: Outphasing power amplifiers," *IEEE Microw. Mag.*, vol. 17, no. 2, pp. 18–31, Feb. 2016.
[5] D. Schreurs, M. O'Droma, A. A. Goacher, and M. Gadringer, *RF Power Amplifier Behavioral Modeling*. New York, NY: Cambridge Univ. Press, 2008.
[6] J. Kim and K. Konstantinou, "Digital predistortion of wideband signals based on power amplifier model with memory," *IET Electron. Lett.*, vol. 37, no. 23, pp. 1417–1418, Nov. 2001.
[7] L. Ding, G. T. Zhou, D. R. Morgan, Z. Ma, J. S. Kenney, J. Kim, and C. R. Giardina, "A robust digital baseband predistorter constructed using memory polynomials," *IEEE Trans. Commun.*, vol. 52, no. 1, pp. 159–165, Jan. 2004.
[8] D. Morgan, Z. Ma, J. Kim, M. Zierdt, and J. Pastalan, "A generalized memory polynomial model for digital predistortion of RF power amplifiers," *IEEE Trans. Signal Process.*, vol. 54, pp. 3852–3860, Oct. 2006.
[9] R. N. Braithwaite, "Wide bandwidth adaptive digital predistortion of power amplifiers using reduced order memory correction," *IEEE MTT-S Int. Microw. Symp. Dig.*, June 2008, pp. 1517–1520.
[10] N. Naraharisetti, C. Quindroit, P. Roblin, S. Gheitanchi, V. Mauer, and M. Fitton, "2D cubic spline implementation for concurrent dual-band system," *IEEE MTT-S Int. Microw. Symp. Dig.*, June 2013, pp. 1–4.
[11] N. Naraharisetti, P. Roblin, C. Quindroit, and S. Gheitanchi, "Efficient least-squares 2-D-cubic spline for concurrent dual-band systems," *IEEE Trans. Microw. Theory Tech.*, vol. 63, no. 7, pp. 2199–2210, July 2015.
[12] L. Miller, *5G RF for Dummies: Qorvo Special Edition*. Hoboken, NJ: John Wiley & Sons, Inc., 2017.
[13] C. de Boor, *A Practical Guide to Splines*, 3rd ed. Wisconsin, USA: Springer-Verlag, 1978.